

Dusty Debris Around Solar-Type Stars: Temporal Disk Evolution

C. Spangler¹ and A. I. Sargent

*Division of Physics, Mathematics and Astronomy, California Institute of Technology,
MS 105-24, Pasadena, CA 91125*

celeste@spanglers.com, afs@astro.caltech.edu

and

M.D. Silverstone², E.E. Becklin, and B. Zuckerman

*Division of Astronomy and Astrophysics, University of California, Los Angeles,
Los Angeles, CA 90095-1562*

murray@as.arizona.edu, becklin@astro.ucla.edu, ben@astro.ucla.edu

ABSTRACT

Using ISO-ISOPHOT we carried out a survey of almost 150 stars to search for evidence of emission from dust orbiting young main sequence stars, both in clusters and isolated systems. Over half of the detections are new examples of dusty stellar systems, and demonstrate that such dust can be detected around numerous stars older than a few $\times 10^6$ years. Fluxes at $60\ \mu\text{m}$ and either 90 or $100\ \mu\text{m}$ for the new excess sources together with improved fluxes for a number of IRAS-identified sources are presented. Analysis of the excess luminosity relative to the stellar photosphere shows a systematic decline of this excess with stellar age consistent with a power law index of -2 .

Subject headings: circumstellar matter — planetary systems — infrared: stars — open clusters and associations

¹present address: 6262 Bothell Cir., San Jose, CA 95123

²present address: Steward Observatory, University of Arizona, Tucson, AZ 85721

1. Introduction

Circumstellar disks are generally accepted as a natural by-product of star formation (e.g. Shu et al. 1993), and there is considerable observational evidence for the presence of such disks around very young solar mass stars (e.g. Sargent 1996, and references therein; Natta, Grinin, & Mannings 2000; Andre, Ward-Thompson, & Barsony 2000; Mundy, Looney, & Welch 2000; Wilner & Lay 2000). The IRAS detection of far infrared radiation from main sequence stars at a level much greater than could be attributed to the stellar photospheres was, nonetheless, unexpected (e.g. Aumann et al. 1984). These stars became known as “Vega-type” stars, after one of the first examples. This infrared excess radiation was interpreted as thermal emission from dust in orbit about the stars (c.f. Backman & Paresce 1993, and references therein; Lagrange, Backman, & Artymowicz 2000). Early coronagraphic observations of scattered light from the Vega-type star β Pictoris indicated an edge-on disk morphology (Smith & Terrile 1984). Recent imaging of thermal emission at mid-IR and mm wavelengths from Vega-type stars, including HR 4796A, MWC 480, and ϵ Eridani, continue to provide support for the disk interpretation (Koerner et al. 1998; Jayawardhana et al. 1998; Holland et al. 1998; Mannings, Koerner, & Sargent 1997; Greaves et al. 1998). Dramatic disk-like images in reflection around HR 4976A and the Herbig Ae/Be star HD 141569 have been recently published (Schneider et al. 1999; Weinberger et al. 1999; Augereau et al. 1999).

Typically, the ages of T-Tauri stars with associated disks are of order 10^6 years old or less. The Vega-type stars have ages ranging from 10^7 to 10^9 years. While known examples of Vega-type systems are fairly well studied, their limited number provides little information on the evolution of circumstellar dust during these later epochs. Yet it is these later epochs that are of critical importance to understanding the development of planetary systems (Lagrange et al. 2000). Gathering a statistical sample of intermediate age objects is difficult. Not only is the time to evolve from proto-planetary to planetary debris disks likely to be brief, but disk emission drops dramatically with age as grains grow and/or dissipate, reducing the emitting surface area. As planetary embryos form close to the stars, the hot inner dust is probably cleared. There are also many mechanisms capable of reorganizing or removing the outer primordial circumstellar dust, including grain growth, Poynting-Robertson drag, and radiation pressure, in times short compared to the ages of older Vega-type stars. In fact, for older stars to exhibit dusty disks there must be an ongoing source of particles; a favored explanation is that some planetesimals are colliding and fragmenting. There is substantial evidence that extrasolar planets are common (Marcy, Cochran, & Mayor 2000), implying smaller planetesimals, collisions of which could provide a reservoir of circumstellar dust, are also common.

Since thermal emission from the little remaining outer, cooler material peaks at wavelengths of $50 - 150 \mu\text{m}$, airborne or space-based instruments are required to detect intermediate age and older disks. However, IRAS, with sensitivities of a few hundred mJy at 60 and $100 \mu\text{m}$, detected only the nearest and brightest disks – mostly those associated with main sequence stars of spectral type A. In addition, the low spatial resolution of IRAS limited the ability to determine if emission was associated with a specific object, particularly at $100 \mu\text{m}$ where galactic cirrus confusion is significant. ISO, with a factor of two improvement in resolution, $46''$ pixels at $60 - 100 \mu\text{m}$, and an order of magnitude increase in sensitivity over IRAS, has expanded our capability to search for circumstellar dust.

Here we describe our ISO program³ of observations to search for dusty circumstellar material, especially around stars of spectral types F and G, and also to study the evolution of disks from the pre-main sequence through the main sequence stages. Details of the target selection are presented in Section 2; an account of observations, data reduction and basic results is given in Section 3; excess radiation calculations are described in Section 4. Results and implications of our observations are discussed in Section 5, and summarized in Section 6.

2. Target Selection

Our targets fell into three distinct categories:

1. Main sequence members of relatively nearby, generally < 120 pc, open clusters including α Persei, Coma Berenices, Hyades, Pleiades, and the Ursa Major nucleus and stream. Cluster ages are between 50 and 700 Myrs and the target stars span spectral types A through K.
2. Selected classical and weak-line T Tauri stars in the Chamaeleon I, Scorpius, and Taurus star forming clouds at ~ 150 pc. Some of these were detected by IRAS but beyond 60 microns only upper limits to the fluxes are available.
3. A small sample of relatively nearby, < 60 pc, isolated stars with indications of youth.

A major problem in defining an evolutionary sequence for circumstellar disk characteristics arises because it is difficult to assign an age to an isolated star. Age determinations rely on a number of factors including the star's position in the HR-diagram, its metallicity, and the

³A NASA/ISO Key Project.

depth of its convection layer. Even with well-defined observable parameters, the calculated age can vary greatly depending on stellar models used. For stars in clusters, a more accurate age determination is possible based on the main sequence turn-off point. By selecting target objects from well-studied clusters, ages are fairly well defined. In order to encompass a variety of evolutionary characteristics in any associated disk, stars in our sample clusters range from the pre-main sequence (PMS), ages $\lesssim 10$ Myr, to the young main sequence, ages up to 1 Gyr. Reasons to include pre-main sequence stars in our study are to establish the initial characteristics of the dusty material whose evolution we wish to understand and to enable an assessment of the fraction of weak-line T Tauri stars (WTTs) which support disks. Weak-line T Tauri stars are similar to classical T Tauri stars (CTTs), but exhibit only weak $H\alpha$ emission and show no other indications of the presence of an accreting disk (Calvet, Hartman, & Strom 2000).

Since the contrast between radiation from the stellar photosphere and the disk increases with longer wavelengths, we confined our search to ISO's 60 and 90/100 μm wavelength bands. IRAS 3σ sensitivity limits at 60 and 100 μm were typically 200 – 300 mJy and 500 – 3000 mJy respectively, depending on the degree of cirrus confusion. Pre-launch sensitivity estimates for ISOPHOT, on which we based our original target selections, were of order 1 mJy (3σ RMS) with a 256 s observation in these bands. Since an F0 V star at 100 pc typically has photospheric fluxes of 3.6 and 1.2 mJy at 60 and 100 μm , respectively, we expected photospheric fluxes characteristic of near-solar-type stars could be detected out to distances of about 100 pc. Beyond this distance and for later-type stars, only fairly strong emission in excess of photospheric values would be detected. Consequently, our candidate open clusters needed to be nearby, $\lesssim 100$ pc. In the late stages of star formation, at ages $\lesssim 50$ Myr, disks are more likely to be brighter and could be detected up to about 200 pc. Our choice of candidate clusters was also constrained by conflicts with ISO Core programs and the ISO pointing restrictions. Complete surveys were out of the question. Nevertheless, the ISO lifetime was sufficient to enable some observations in all clusters we considered interesting.

Table 1 lists the clusters from which we selected targets, along with their ages, distances, the number of targets observed, observing modes, and integration times.

Target stars in the young open clusters were selected from lists of cluster members published by Prosser (1992) for α Persei, by Boesgaard (1987) and Bounatiro (1993) for Coma Berenices, by Schwan (1991) for the Hyades, by Soderblom et al. (1993a) for the Pleiades, and by Boesgaard, Budge, & Burck (1988), Soderblom & Clements (1987) and Soderblom et al. (1993b) for Ursa Major. Within each cluster, preference was given to targets with relatively low cirrus confusion, as determined from the IRAS Sky Survey

background measurements. In Coma Berenices, a sparse cluster with few confirmed members and relatively low cirrus, we included nearly all dwarf stars with spectral types later than A0. By including all possible Ursa Major candidates not reserved by ISO core programs, we sampled a wide range of spectral types in this cluster, from early A to early K, although most objects are of spectral types F and G. For the remaining clusters where there were larger numbers of candidates available, we gave preference to stars with spectral types near solar, mostly late F- and G-type stars. When choosing targets in the Hyades, we also took into account indications of potential far infrared excesses based on IRAS 12 and 25 μm data. Binarity was not a cause for exclusion from our sample because we hoped to increase understanding of the relationship between circumstellar dust and multiplicity. Finally, we made efforts to include targets with a range of rotational velocities to assess the relationship between the presence of a disk and stellar rotation.

Very young stars included CTTs and WTTs in the Chamaeleon I association selected from the published lists of Gauvin & Strom (1992) and Alcalá et al. (1995), WTTs in Taurus from Wichmann et al. (1996), and WTTs in the Upper Scorpius association from Walter et al. (1994). In Chamaeleon I, most sources have measured IRAS fluxes at 12 and/or 25 μm but lack good quality measurements at 60 and/or 100 μm . Other WTTs were selected to span the range of the limited age estimates available, and for lower cirrus confusion.

We also included 19 field stars (hereafter referred to as Young Field Stars) which exhibited indications of youth, primarily based on published chromospheric activity age indicators. We intended to limit distances to less than 60 pc, but following the publication of Hipparcos data it became clear that two observed stars are actually more distant than this cutoff. Like the cluster stars, the Young Field Stars span the age range 60 to 800 Myr with a median of 180 Myr. They encompass spectral types A through K, but are concentrated on spectral types F and G. Individual stellar ages are presented in Table 2.

3. Observations and Results

We selected the ISOPHOT C100 detector (Lemke et al. 1996) for our target observations. Targets were observed throughout the ISO mission, and our observing strategies changed as our understanding of ISOPHOT performance improved. The first group of 63 observations was made between 1996 June and 1996 December. The majority employed the 60 and 100 μm filters and the triangular chopping mode with a 150 arcsec throw. Eight stars in Coma Berenices (see Table 3) were observed with a “staring chain” – an on-target observation followed by a background observation 3 arcmin north of the target, then the next on-target observation, etc., first in the 60 μm filter, then in the 100 μm filter. The

second group of 85 observations was made between 1997 June and 1998 March using the 60 and 90 μm filters and the raster mode in a 3×3 grid with 46 arcsec steps. A list of total integration times and number of targets observed in each cluster is presented in Table 1.

Data reduction made use of the ISOPHOT Interactive Analysis (PIA) package version 7.3 (Gabriel et al. 1997) and was supported by our own routines. Our final results are based on data from Off-Line Processing (OLP) version 7.0. Standard reduction parameters were used for linearization of ramps, 2-threshold deglitching, first-order polynomial voltage ramp fitting, and reset interval correction. Slope deglitching was slightly modified by using a sigma range of 2.4 and max/min clipping. Chopped observations were corrected with the default chopper-loss factors given by the ISOPHOT Team (Gabriel et al. 1997). Dark-current subtraction employed the orbital-dependent model values. Finally, to limit the influence of the non-linear response of the detector to a change in flux, we discarded the first third of each raster pointing.

We calibrated the data with the on-board Faint Calibration Source (FCS) measurements. Since there is significant evidence for detector drifts during observation, the best strategy obtains calibration measurements immediately before and after a target observation. For the staring and chopped observations, which were all made before the detector drift was well understood, FCS measurements were made at the beginning and end of a group of individual observations. Calibration factors were then interpolated for each target and background observation. For raster observations, FCS measurements were made immediately before and after each target observation and calibration factors interpolated at each raster step. The application of the FCS calibration also removes a first order flat-field. Residual effects exist, but in general their magnitude is less than the other observational uncertainties. As far as possible, these FCS-based calibrations were cross-checked by comparing the method of calibration from the observed ISO and published IRAS backgrounds and a number of actual IRAS source measurements as described by Silverstone, Becklin, & Spangler (1998), Silverstone (2000) and Spangler et al. (1999) and were found to be consistent. A more detailed discussion of the calibration comparisons is given in Appendix A. We are confident the PIA calibration using the FCS measurements is sufficiently reliable to support our conclusions. Corrections for the point-spread function (PSF) were applied using model calculations which give the fraction flux falling on the center pixel of the array as 0.66, 0.57 and 0.54 at 60, 90 and 100 μm , respectively (Laureijs 1999)⁴. A more detailed discussion of the standard data reduction procedures is presented by Silverstone (2000).

For all observing strategies used here, a source was considered detected if the flux at the

⁴Article available at http://www.iso.vilspa.esa.es/users/expl_lib/PHT_list.html

on-target (center) pixel exceeded three times the standard deviation of the flux on the eight surrounding pixels. This provided a conservative approach to problematic observations. In all cases, the standard deviation of the flux on the surrounding pixels is higher than any other statistical uncertainties associated with the observation. In five cases – all in the Chamaeleon and Scorpius clusters – the source was extended to one outer pixel. This pixel was excluded from the calculation of the background standard deviation. At both $60\ \mu\text{m}$ and $100\ \mu\text{m}$, typical 3σ noise limits for chopped observations were 100 mJy in 256 s. For raster observations, corresponding limits were 50 mJy at $60\ \mu\text{m}$ and 40 mJy at $90\ \mu\text{m}$ in 473 s. In regions of very low cirrus, the noise limits were as much as a factor of three lower. Conversely, in regions with high cirrus confusion, the noise limits were as much as a factor of five higher. These sensitivities are much worse than originally anticipated and, as a result, the detection of excesses was somewhat compromised. A complete list of all observed targets with signals and uncertainties is presented in Table 3 and Table 4.

A total of 36 targets were detected out of 148 observed. One-third of the detections are in the young Chamaeleon cluster.

4. IR Excesses

In order to determine if there is excess emission at the wavelengths observed, a good estimate of the stellar photospheric flux is required. For non-PMS cluster members more distant than the Hyades (46 pc), the photospheric contributions at 60, 90 and $100\ \mu\text{m}$ are negligible compared to the measured ISOPHOT sensitivities (see Section 3). For stars in the Hyades and closer and PMS stars, we estimated the photospheric flux from published K-band magnitudes (Alcala et al. 1995; Gauvin & Strom 1992; Lawson, Feigelson, & Huenemoerder 1996; Randich, Schmitt, & Prosser 1996; Walter et al. 1994). Several K-band magnitudes were also obtained for us by J. Hare (1997, private communication). Where K-band magnitudes were unavailable, we used V-band magnitudes and published V-[12] colors (Cohen et al. 1987). A comparison of the results of these two extrapolation methods suggests the uncertainty in the predicted photospheric values is less than 10%, significantly less than the noise in our measurements.

Of our 36 detected sources, 33 show evidence of excess far-infrared emission. Basic characteristics of these excess sources including spectral type, V-band magnitude, B-V color, effective temperature, rotational velocity, distance, age and multiplicity are listed in Table 5.

About one-third of these sources are in young star forming regions and, based on IRAS results, were suspected to have infrared excesses. For the most part, only the 12 and $25\ \mu\text{m}$

IRAS measurements are reliable and our new measurements at 60 and 100 μm complement these. Our ISO observations demonstrate for the first time that there is excess emission at 60 μm and 90 or 100 μm for thirteen cluster stars, five Young Field Stars and one other field star. These excess sources are presented in Tables 6 (CTTs and WTTs) and 7 (cluster and field stars) together with IRAS measurements and upper limits.

The detections of infrared excess are associated with stars of a range of spectral types and luminosities. For convenience we adopt a parameter that is independent of luminosity to describe systems exhibiting excess emission from circumstellar dust. The fractional excess luminosity, $f_d \equiv L_{\text{ex}}/L_\star$, where L_{ex} is the luminosity of dust and L_\star is the stellar bolometric luminosity, effectively provides a measure of the relative dust mass for small particles of radius $a \lesssim 1\mu\text{m}$ in systems with roughly the same dominant temperature. Values of f_d for each of our excess sources were calculated following the method of Backman & Gillett (1987), summing the luminosities in each wavelength band and including a correction to account for excess flux from wavelengths longer than the 90 or 100 μm band: $f_d = [L_{\text{ex}(12)} + L_{\text{ex}(25)} + L_{\text{ex}(60)} + L_{\text{ex}(90 \text{ or } 100)} + c]/L_\star$.

IRAS 12 and 25 μm measurements, where available, were used to determine $L_{\text{ex}(12)}$ and $L_{\text{ex}(25)}$. However, for the vast majority of our targets older than ~ 20 Myr, there was either no measurable excess emission at 12 μm and 25 μm or no flux measurements available. Values for $L_{\text{ex}(60)}$ and $L_{\text{ex}(90 \text{ or } 100)}$ were derived from the data in Tables 6 and 7. To account for any unmeasured excess emission at wavelengths shorter than 60 μm and longer than 100 μm , we used the values of f_d and the 25, 60 and 100 μm measurements for 14 stars from Table X in Backman & Paresce (1993) and calculated the correction factor necessary to reproduce the final f_d s from only the 60 and 100 μm excesses. This correction factor, $c = 1.85$, was then applied where we had only 60 μm and 90 or 100 μm data.

5. Discussion

5.1. Cluster Stars

We detected at least one infrared excess source in almost every cluster observed. Since the implications of the detections differ by cluster, we review each cluster separately.

Coma Berenices: Three IR-excess sources were detected out of 26 stars observed. While the actual number of detections is small, several characteristics of the cluster and the observations combine to make this a remarkable result. Coma Berenices is a very sparse cluster, comprised of only 42 optically identified members at the time of our observations, 35 of which are of spectral type earlier than K0. It is one of the oldest open clusters we observed,

with an age of 500 Myr. Based on the drop off of f_d with age described below in Section 5.3, Coma Berenices stars should have values of f_d on average a factor of 100 less than stars in the α Persei cluster. The fact that Coma Berenices at 88 pc is relatively close increases our sensitivity to excess flux there compared to α Persei by a factor of only four. Furthermore, this cluster could be observed only early in ISO’s lifetime when we used the less-sensitive chopping mode with 3σ noise limits at least four times higher than those of the raster observations. For the three Coma Berenices excess sources to be detectable, they must have values of f_d 10 to 100 times higher than we would expect, indicating they are unusual systems. At least three other stars in the cluster display only slightly less than 3σ signals on the center pixel, suggesting the presence of additional excess systems. Only very limited information on the members of Coma Berenices is available. Detailed photometric and spectroscopic observations and FIR data are nearly non-existent, although there are now Two Micron All Sky Survey (2MASS) observations.

Ursa Major: Our observations provide the first firm evidence for substantial excesses around stars in the Ursa Major cluster, which has an age ~ 300 Myr and lies at a distance ~ 25 pc. This cluster has two components: the nucleus and stream (Roman 1949). Searches to date, generally involving only the A-type members (Abraham et al. 1998; Lecavelier Des Etangs, Ferlet, & Vidal-Madjar 1997; Skrutskie et al. 1991), produced evidence for only one circumstellar disk – associated with β UMa, a nucleus member – out of 30 separate nucleus and stream systems observed. One of our detected stars, HD 139798, was suggested as a $25\ \mu\text{m}$ excess source by Stencel & Backman (1991), but its status as a possible Ursa Major stream member was not noted. All of our detected excess sources are probable members of the Ursa Major stream. However, all of our observations of the nucleus stars were made early in the ISO mission and used the chopping mode, with the lower sensitivity as mentioned above. Two nucleus stars exhibited emission at a level just less than our 3σ limit indicating that more sensitive long wavelength observations may reveal additional excess systems.

Pleiades: Here we detected two very bright sources out of fourteen stars observed. While these two excess sources are intriguing they are not likely to be typical. Considering the relatively young age of the Pleiades, just over 100 Myr, we might expect a large number of sources with $f_d \sim 10^{-4}$. However, for a G5 star, the median spectral type observed in this cluster, the lowest detectable f_d was $\sim 7 \times 10^{-4}$. With decreased sensitivity in many regions of this cluster due to high cirrus, it is not surprising we detected only the highest- f_d disks. We note that, due to ISO’s pointing constraints, there was very limited time to observe the Pleiades resulting in a survey of only a tiny fraction of its members. The potential for detecting additional excess sources in this cluster is high.

Chamaeleon I and Upper Scorpius: Perhaps the least surprising of the detections are

those of the PMS stars in the Chamaeleon I and Upper Scorpius associations. We were able to detect emission from 14 of 33 observed targets. While the vast majority (13) of the detected stars were known previously to be excess sources, most lacked reliable 60 and/or 100 μm fluxes, or were confused with other sources. Unfortunately, the resolution of ISO was insufficient to resolve three of the CTTs we observed. We detected excess in five of the WTTs we observed. All of the non-detected targets are WTTs, and are either highly variable (e.g. VX Cha) or are from the X-ray detected PMS sources (Alcala et al. 1995), many of which were determined to be older stars after our program of observations was executed. Comments on individual sources are in notes to Table 6. Of the two stars observed in Upper Scorpius, one resulted in a very strong detection, over 100 mJy in both the 60 and 90 μm bands. The similarity in appearance to the Chamaeleon sources suggests there are likely to be numerous excess sources in this cluster yet to be identified. In fact, Backman et al. (1998) reported a significant detection of the sum of emission from 6 A-type stars in the Sco-Cen association.

α Persei: In contrast to the preceding clusters, the detection rate in this cluster was disappointing. With an estimated age ~ 50 Myr, α Persei would be expected to contain systems with $f_d \sim 10^{-3}$. Observations of this cluster are complicated by confusion with galactic plane sources as well as a greater distance of 185 pc. Nevertheless, an $f_d \sim \text{few} \times 10^{-4}$ for an F5 star, the median observed spectral type of this cluster, would be well within our detection limits. However, recent dating of this cluster by lithium depletion boundary methods (Stauffer et al. 1999) yields an age of ~ 125 Myr, more than double the previous estimate. This would reduce our expected f_d by a factor of four, putting the brighter cluster systems just at our detection limit. If α Persei is as young as first thought, it would be one of the few clusters with ages just older than those of the WTTs, such as in Chamaeleon and Taurus, making it extremely important for characterizing circumstellar disks at this point in their evolution. More sensitive observations and a resolution of the age question are essential for this cluster.

Taurus: The lack of significant detections in Taurus is also surprising. With an average age of about 25 Myr and at 140 pc, Taurus is comparable to the Chamaeleon cluster, and thus would be expected to contain a large number of detectable excess sources. But time to observe this cluster was limited and thus statistics are poor. The targets observed were X-ray selected WTTs; however, unlike those in Chamaeleon, most Taurus WTTs are confirmed PMS stars (Bouvier et al. 1997).

Hyades: This cluster, one of the older clusters at 625 Myr, is relatively close at only 46 pc. This is about twice as far and twice as old as the Ursa Major cluster, where our detected f_d s are on the order of 10^{-4} . For the Hyades we expect f_d to be on the order

of 10^{-5} , right at our detection limit for an F5 star, the median spectral type observed in the Hyades. Thus, typical disks could have escaped detection. Again, observing time on this cluster was limited and we observed only a small percentage of cluster members. More sensitive observations are necessary to determine the true incidence of infrared excess.

5.2. Young Field Stars

For most of these stars, ages were taken from the literature (see Table 2). In a few cases, ages were unavailable or unconfirmed. Chromospheric activity is a useful age-indicator for young, low-mass stars and can be measured by the brightness of the Ca-II core reversal. This reversal is often measured by the so-called S-parameter (Duncan, et al. 1991; Henry et al. 1996, and references therein). The S-parameters for two stars, HD 35850 and HD 209253 were measured with the 0.6-m Coude Auxiliary Telescope and the Hamilton Echelle Spectrograph at Lick Observatory by Silverstone (2000). These data were calibrated by measuring stars in common with Duncan, et al. (1991) and Henry et al. (1996). Ages (Table 2) were calculated following the method of Duncan, et al. (1991).

Among the Young Field Stars, we find detectable excesses in seven out of the nineteen stars observed. The values of f_d for these excess stars are comparable to those of some members of the open clusters, but distances to these two samples are very different. On average, the Young Field Stars are at 45 pc, and have an age of 200 Myr, making them most analogous to the Ursa Major cluster, where there was also a significant number of detections. A greater percentage of Young Field Star observations than the Ursa Major observations used the high-sensitivity raster mode.

The S-parameter was also measured for the star HD 151044, an Ursa Major Stream candidate ($\approx 300 \times 10^6$ yrs) (Boesgaard et al. 1988). However its membership has been questioned on the basis of relatively low chromospheric emission and similar but not entirely consistent space motion with the Ursa Major Stream (Soderblom & Clements 1987; Soderblom & Mayor 1993). Our new chromospheric activity age, 2.8×10^9 yrs, is consistent with HD 151044 being too old to be part of the Ursa Major Stream. However, the calculated excess seems extreme if the star is so old.

5.3. The Age– f_d Correlation

As defined above, f_d is the fractional dust luminosity, L_{ex}/L_{\star} . For each cluster and for the Young Field Stars as a whole, an average f_d was calculated as follows: the sum of

all values for f_d from detections and non-detections, including negative values, was divided by the total number of targets observed. Negative values for f_d result when the observed flux was less than the photospheric flux estimate and in all the approximately 40 cases, the “negative excess” was less than the 3σ noise level. The Chamaeleon I sources were separated into two groups because of the wide relative age spread of the stars. The division was set at 10 Myr, resulting in groups of nearly equal size. However, whether Chamaeleon I is plotted as one group or two, the effect on the fitted age– f_d relation is negligible.

Figure 1 shows the averaged f_d s versus the cluster ages. Comparable values for a few nearby Vega-type stars are plotted over the main cluster results in Figure 2. There is clear evidence for a systematic decrease in the fractional infrared excess emission with stellar age. A regression fit to the cluster data yields a reasonably good fit with a power-law of the form $f_d \propto (\text{age})^{-1.76}$. This is consistent with submillimeter studies of Pleiades, Ursa Major, Taurus and field stars by Zuckerman & Becklin (1993), who found $\text{DustMass} \propto (\text{age})^{-2}$. In contrast, Habing et al. (2000) have recently proposed that the majority of circumstellar disks disappear after the first 400 Myr based on their detection of only a few disks around field stars with ages greater than 400 Myr. While it is difficult to compare the two sets of observations directly because of differing target samples and noise levels, we detect excess emission from dust around seven stars with ages greater than 400 Myr, showing disks do persist beyond 400 Myr though the amount of dust tends to decline.

Since f_d is a measure of the emission from circumstellar dust, it should be correlated with the mass of dust (see also Zuckerman & Becklin 1993). Silverstone (2000) provides an approximate conversion relation, dust mass = $f_d \times 1.4 \times 10^4 M_{\text{moon}}$, where M_{moon} is the mass of the moon. Masses calculated in this way lead to the right-hand axis in Figure 1.

The power-law index near -2 in the age–dust mass relationship can possibly be explained by a simple model of collisionally replenished secondary dust disks. If the dust clearing time scale is shorter than the age of the system, the amount of secondary dust will be determined by the instantaneous collisional rate of large particles. The typical dust clearing time scales are given by Backman & Paresce (1993) and Silverstone (2000) and are less than 10^7 years. The collisional rate of large particles dN/dt should go as N^2 where N is the number density of large planetesimals, comets or asteroids in the system. Thus

$$f_d \propto \frac{dN}{dt} \propto -N^2. \quad (1)$$

In addition, it is expected that the loss of large particles will be determined by the same collisional type process such that integrating equation 1 we find that the number of large particles will decrease with time as

$$N \propto \frac{1}{t}. \quad (2)$$

Combining equations 1 and 2, we get that the mass of emitting dust is given by

$$M(\text{emitting dust}) \propto f_d \propto \frac{dN}{dt} \propto N^2 \propto \frac{1}{t^2}. \quad (3)$$

This is similar to the observed power law fall off. The problem can also be reversed. The fact that we observe the mass of emitting dust dropping off as $1/t^2$ suggests that in this model, the number of large particles N , in planetesimals, comets and asteroids, falls as $1/t$ independent of the mechanism that produces the fall off.

5.4. Correlations with other stellar characteristics

With only a small number of detections in each cluster, it is difficult to draw general conclusions regarding the relationship between circumstellar material and stellar characteristics such as multiplicity and rotation. We detected dust around single stars, several spectroscopic binaries including all three Coma Berenices excess stars and one Young Field Star, HD 177996, and one wide binary, HD 125451 (separation ~ 4000 AU). Therefore, over the age range of 10 to 600 Myr the presence of a stellar companion does not necessarily preclude the existence of associated circumstellar material. Osterloh & Beckwith (1995) and Jensen et al. (1996) show that disks may surround members of binary systems in cases where the separation is either less than 1 AU, or greater than 100 AU.

The detected sources exhibit a wide range of rotational velocities. In the young open clusters, half our detected excess sources have $v \sin i$ less than the median rotational velocity of their parent clusters. This distribution is similar to the $v \sin i$ distribution in the original sample of targets. In each cluster about half of the targets had $v \sin i$ less than the median rotational velocity of the cluster. Only in the Pleiades is there a significant imbalance; there the two detected sources have the highest $v \sin i$ of the stars we observed in that cluster, roughly five times the cluster median. Among the Young Field Stars, those detected have a range of rotational velocities similar to the young open clusters (including both slow rotators, and stars with rotational velocities similar to the two detected Pleiades stars). A dearth of comprehensive data for rotational velocities of the PMS stars in Scorpius and Chamaeleon I prevents detailed discussion for these samples.

Most of our detections in the young open clusters and Young Field Stars (i.e. not PMS stars) are stars of spectral type F. This is partly due to selection effects: we observed a large

fraction of F-type stars and dust around F-type stars would be easier to detect because of the higher luminosity than G- or K-type stars. For F-type stars alone, we detect excess IR emission in 12 out of 48 stars observed, or 25%. In their review, Lagrange et al. (2000) state for stars of spectral types A–K the fraction with disks is 15%. While the fraction for F-type stars specifically is not noted, our results suggest the fraction is indeed significantly higher than 15%. Our results also indicate that future work is likely to confirm a similarly higher percentage for G- and K-type stars.

6. Summary

A survey of almost 150 pre-main sequence and young main sequence stars, the majority of which are members of young open clusters, has been carried out with ISOPHOT. Excess emission at 60, 90, and/or 100 μm , presumably from circumstellar debris disks, has been detected from 33 of the observed stars. The detections are distributed among the observed clusters/groups. Twenty of the stars, most of which are of spectral type F, were not previously known to exhibit excess emission, and represent a new set of Vega-type systems. Other ISO programs of observations with similar objectives to ours (Robberto et al. 1999; Habing et al. 2000) have resulted in much lower detection rates. Much of this can be attributed to greatly different observing strategies, including shorter integration times, method of measuring background, and choice of targets. Because of the differences in observational techniques, it is difficult to compare the results.

A major conclusion from our observations is how the excess IR emission evolves with time. The ratio of excess IR luminosity to stellar luminosity, f_d , appears to drop off with age according to the power law $f_d \propto (\text{age})^{-1.76}$. A power law $\propto (\text{age})^{-2}$ is expected for collisionally replenished secondary dust disks. We do not see evidence for an abrupt cessation of the debris disk phenomenon as reported by Habing et al. (2000).

The detection of the new IR excess sources reported here is only the beginning. More work needs to be done to help characterize the spectral and spatial extent of systems which have been detected. We have no 100 μm measurements for any of the young cluster stars which we observed in the chopping mode. Many of the PMS objects we measured at 100 μm are not well characterized spatially. We expect that the DEep Near Infrared Survey of the Southern Sky (DENIS) and 2MASS searches will add near-IR data to many of the young cluster sources, but may not be able to measure some of the more distant stars. Observations of our new excess sources are also needed in the 10 – 60 μm region. However, the far infrared wavelengths at which dust disks are most readily studied are inaccessible from the ground, requiring future high-altitude and space missions, such as SOFIA and SIRTf. Finally, the

multiplicity of a number of these sources, both young cluster and PMS, needs to be better established.

Our results indicate that there is great potential for more sensitive space-based studies of clusters to identify additional solar-type stars with far-infrared excess. The detection and analysis of many more of these intriguing objects will provide a better understanding of the planet formation process.

The ISOPHOT data presented in this paper were reduced using PIA, which is a joint development by the ESA Astrophysics Division and the ISOPHOT consortium. This work was facilitated by the use of the Vizier service and the SIMBAD database developed at CDS. This work has made use of XCATSCAN, an internet service provided by the Infrared Processing and Analysis Center (IPAC), which is operated by the Jet Propulsion Lab and the California Institute of Technology under contract to NASA. We would like to thank M. Jura and P. Goldreich for assistance with the original ISO program, and D. Backman for helpful comments. This research was supported in part by JPL Subcontract No. 1201061 pursuant to JPL NASA Prime Contract Task Order No. N1260.

A. Flux Calibration

As discussed by Spangler et al. (1999) and Silverstone (2000), a number of targets from our entire ISO:DEBRIS program had existing IRAS Faint Source Catalogue (FSC) measurements at $60\ \mu\text{m}$ that were confirmed to be stellar in origin. We made use of these data to check the PIA/FCS calibration of our ISOPHOT fluxes. The comparison of 24 sources is plotted in Figure A1 along with the line $F_{ISO} = F_{IRAS}$ for reference, and shows good agreement between the IRAS FSC and ISO FCS flux measurements.

REFERENCES

- Abraham, P., Leinert, C., Burkert, A., Lemke, D., & Henning, T. 1998, *A&A*, 338, 91
- Alcala, J. M., Krautter, J., Schmitt, J. H. M. M., Covino, E., Wichmann, R., Mundt, R. 1995, *A&AS*, 114, 109
- Alcala, J. M., Krautter, J., Covino, E., Neuhauser, R., Schmitt, J. H. M. M., & Wichmann, R. 1997, *A&A*, 319, 184

- Andre, P., Ward-Thompson, D., & Barsony, M. 2000, in *Protostars and Planets IV*, ed. V. Mannings, A. P. Boss, & S. S. Russell (Tucson: University of Arizona Press), 59
- Augereau, J. C., Langrange, A. M., Mouillet, D., & Menard, F. 1999, *A&A*, 350, 51L
- Aumann, H. H. et al. 1984, *ApJ*, 278, 23
- Backman, D. E., Fajardo-Acosta, S. B., Stencel, R. E., & Stauffer, J. R. 1998, *Ap&SS*, 255, 91
- Backman, D. E., & Gillett, F. C., 1987, in *LNP 291, Cool Stars, Stellar Systems and the Sun*, ed. J. L. Linsky & R. E. Stencel (Berlin: Springer-Verlag), 340
- Backman, D. E., & Paresce, F. 1993, in *Protostars and Planets III*, eds. E. H. Levy & J. I. Lunine (Tucson: University of Arizona Press), 1253
- Barrado y Navascues, D., Stauffer, J. R., Song, I., & Caillault, J.-P. 1999, *ApJ*, 520, 123
- Boesgaard, A. M. 1987, *ApJ*, 321, 967
- Boesgaard, A. M., Budge, K. G., & Burck, E. E. 1988, *ApJ*, 325, 749
- Bounatiro, L. 1993, *A&ASS*, 100, 531
- Bouvier, J. et al. 1997, *A&A*, 318, 495
- Calvet, N., Hartmann, L., & Strom, S. E. 2000, in *Protostars and Planets IV*, ed. V. Mannings, A. P. Boss, & S. S. Russell (Tucson: University of Arizona Press), 377
- Cambresy, L., Copet, E., Epchtein, H., De Batz, B., Borsenberger, J., Fouque, P., Kimeswenger, S., & Tiphene, D. 1998, *A&A*, 338, 977
- Cohen, M., Schwartz, D. E., Chokshi, A., & Walker, R. G. 1987, *AJ*, 93, 1199
- Covino, E., Alcalá, J. M., Allain, S., Bouvier, J., Terranegra, L., & Krautter, J. 1997, *A&A*, 328, 187
- Duncan, D. K. et al. 1991, *ApJS*, 76, 383
- Eggen, O. 1973, *PASP*, 85, 381
- Favata, F., Barbera, M., Micela, G., & Sciortino, S. 1993, *A&A*, 277, 428
- Feigelson, E. D., Casanova, S., Montmerle, T., & Guibert, J. 1993, *ApJ*, 416, 623

- Gabriel, C., Acosta-Pulido, J., Heinrichsen, I., Morris, H., & Tai, W.-M. 1997, in ASP Conf. Ser. 125, *Astronomical Data Analysis Software and Systems VI*, ed. G. Hunt & H. E. Payne (San Francisco: BookCrafters, Inc.), 6, 108
- Gauvin, L. S., & Strom, K. M. 1992, *ApJ*, 385, 217
- Greaves, J. S. et al. 1998, *ApJ*, 506, 133
- Griffin, R. F. 1992, *The Observatory*, 112, 41
- Habing, H. J. et al. 2000, *A&A*, in press
- Hartigan, P. 1993, *AJ*, 105, 1511
- Heckmann, O., Dieckvoss, W., & Kox, H. 1956, *Astr. Nach.*, 283, 109
- Henning, Th., Pfau, W., Zinnecker, H., & Prusti, T. 1993, *A&A*, 276, 129
- Henry, G. W., Fekel, F. C., & Hall, D. S. 1995, *AJ*, 110, 2926
- Henry, T. J., Soderblom, D. R., Donahue, R. A., & Baliunas, S. L. 1996, *AJ*, 111, 439
- Hertzprung, E. 1947, *Ann. Leiden Obs.*, Vol. 19, No. 1A
- Holland, W. S. et al. 1998, *Nature*, 392, 788
- Jayawardhana, R., Fisher, S., Hartmann, L., Telesco, C., Pina, R., & Fazio, G. 1998, *ApJ*, 503, 79.
- Jeffries, R. D. 1995, *MNRAS*, 273, 559
- Jensen, E. L. N., Mathieu, R. D., & Fuller, G. A. *ApJ*, 458, 312
- Jura, M., Malkan, M., White, R., Telesco, C., Pina, R., & Fischer, R. S. 1998, *ApJ*, 505, 897
- Kenyon, S. J., Dobrzycka, D., & Hartmann, L. 1994, *AJ*, 108, 1872
- Koerner, D. W., Ressler, M. E., Werner, M. W., & Backman, D. E. 1998, *ApJ*, 503, 83
- Lagrange, A.-M., Backman, D. E., & Artymowicz, P. 2000, in *Protostars and Planets IV*, ed. V. Mannings, A. P. Boss, & S. S. Russell (Tucson: University of Arizona Press), 639
- Laureijs, R. J. 29 June 1999, *Point Spread Function Fractions Related to the ISOPhot C100 and C200 Arrays Version 1.0*

- Lawson, F. A., Feigelson, E. D., & Huenemoerder, D. P. 1996, *MNRAS*, 280, 1071
- Lecavelier Des Etangs, A., Ferlet, R., & Vidal-Madjar, A. 1997, *A&A*, 328, 602
- Lemke, D. et al. 1996, *A&A*, 315, L64
- Marcy, G. W., Cochran, W. D., & Mayor, M. 2000, in *Protostars and Planets IV*, ed. V. Mannings, A. P. Boss, & S. S. Russell (Tucson: University of Arizona Press), 1285
- Mannings, V., Koerner, D. W., & Sargent, A. I. 1997, *Nature*, 388, 555
- Mantegazza, L., Poretti, E., Antonello, E., & Bossi, M. 1992, *A&A*, 256, 459
- Meynet, G., Mermilliod, J.-C., & Maeder, A. 1993, *A&AS*, 98, 523
- Mundy, L. G., Looney, L. W., & Welch, W. J. 2000, in *Protostars and Planets IV*, ed. V. Mannings, A. P. Boss, & S. S. Russell (Tucson: University of Arizona Press), p. 355
- Natta, A., Grinin, V. P., & Mannings, V. 2000, in *Protostars and Planets IV*, ed. V. Mannings, A. P. Boss, & S. S. Russell (Tucson: University of Arizona Press), p. 559
- Odenkirchen, M., Soubiran, C., & Colin, J. 1998, *NewA*, 3, 583
- Osterloh, M., & Beckwith, S. V. W. 1995, *ApJ*, 439, 288
- Perryman, M. A. et al. 1998, *A&A*, 331, 81
- Preibisch, T., & Zinnecker, H. 1999, *AJ*, 117, 2381
- Prosser, C. F. 1992, *AJ*, 103, 488
- Prusti, T., Whittet, D. C. B., & Wesselius, P. R. 1992, *MNRAS*, 254, 361
- Randich, S., Schmitt, J. H. M. M., & Prosser, C. 1996, *A&A*, 313, 815
- Robberto, M., Meyer, M. R., Natta, A., & Beckwith, S. V. W. 1999, in *ASP Conf. Ser. 427, The Universe as Seen by ISO*, eds. P. Cox & M. F. Kessler, 195
- Robichon, N., Arenou, F., Mermilliod, J.-C., & Turon, C. 1999, *A&A*, 345, 471
- Roman, N. *ApJ*, 110, 205
- Sargent, A. I. 1996, *IAUS*, 170, 151
- Schneider, G. et al. 1999, *ApJ*, 513, 127

- Schwan, H. 1991, *A&A*, 243, 386
- Skrutskie, M. F., Snell, R., Dutkevitch, D., Strom, S. E., Schloerb, F. P., & Dickman, R. L. 1991, *AJ*, 102, 1749
- Shu, F., Najita, J., Galli, D., Ostriker, E., & Lizano, S. 1993, in *Protostars & Planets III*, eds. E. H. Levy & J. I. Lunine (Tucson: University of Arizona Press), 3
- Silverstone, M. 2000, Ph.D. thesis, UCLA
- Silverstone, M., Becklin, E. E., & Spangler C. 1998, *Ap&SS*, 255, 119
- Smith, B. A., & Terrile, R. J. 1984, *Science*, 226, 1421
- Soderblom, D. R., & Clements, S. D. 1987, *AJ*, 93, 920
- Soderblom, D. R., & Dappen, W. 1989, *ApJ*, 342, 945
- Soderblom, D. R., Jones, B. F., Balachandran, S., Stauffer, J. R., Duncan, D. K., Fedele, S. B., & Hudon, J. D. 1993a, *AJ*, 106, 1059
- Soderblom, D. R., & Mayor, M. 1993, *AJ*, 105, 226
- Soderblom, D. R., Pilachowski, C. A., Fedele, S. B., & Jones, B. F. 1993b, *AJ*, 105, 2299
- Soderblom, D. R., King, J. R., & Henry, T. J. 1998, *AJ*, 116, 396
- Spangler, C., Silverstone, M. D., Becklin, E. E., Hare, J., Zuckerman, B., Sargent, A., & Goldreich, P. 1999, in *ASP Conf. Ser. 427, The Universe as Seen by ISO*, eds. P. Cox & M. F. Kessler, 405
- Stauffer, J. R. et al. 1999, *ApJ*, 527, 219
- Stauffer, J. R., Hartmann, L. W., & Burnham, J. N. 1985, *ApJ*, 289, 247
- Stencel, R. E., & Backman, D. E. 1991, *ApJS*, 75, 905
- Walter, F. M. 1992, *AJ*, 104, 758
- Walter, F. M., Vrba, F. J., Mathieu, R. D., Brown, A., & Myers, P. C. 1994, *AJ*, 107, 692
- Weaver, Wm. B., & Jones, G. 1992, *ApJ*, 78, 239
- Weinberger, A. J., Becklin, E. E., Schneider, G., Smith, B. A., Lowrance, P. J., Silverstone, M. D., Zuckerman, B., & Terrile, R. J. 1999, *ApJ*, 525, 53

Wichmann, R. et al. 1996, A&A, 312, 439

Wilner, D. J., & Lay, O. P. 2000, in Protostars and Planets IV, ed. V. Mannings, A. P. Boss,
& S. S. Russell (Tucson: University of Arizona Press), 509

Zuckerman, B., & Becklin, E. E. 1993, ApJ, 414, 793

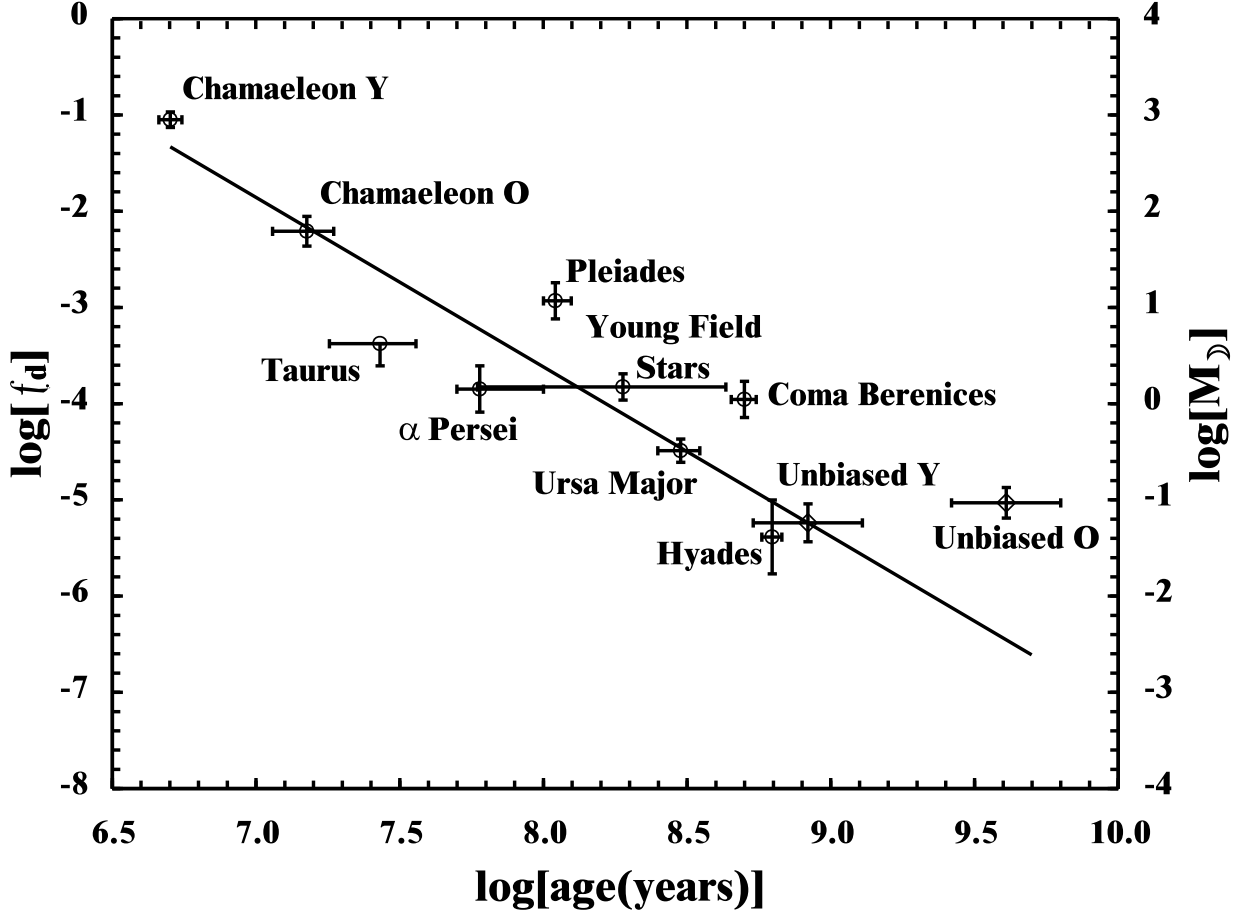


Fig. 1.— The behavior of f_d with stellar age. Cluster ages are taken from the literature (see Table 1). The plotted line is a regression fit to the data with slope $\approx -1.76y$. Plotted points represent an average f for each cluster that includes both detections and non-detections. Vertical error bars represent the standard deviation of the average. The two points, Unbiased Y and Unbiased O are from Silverstone (2000) and are not included in the calculation of the regression.

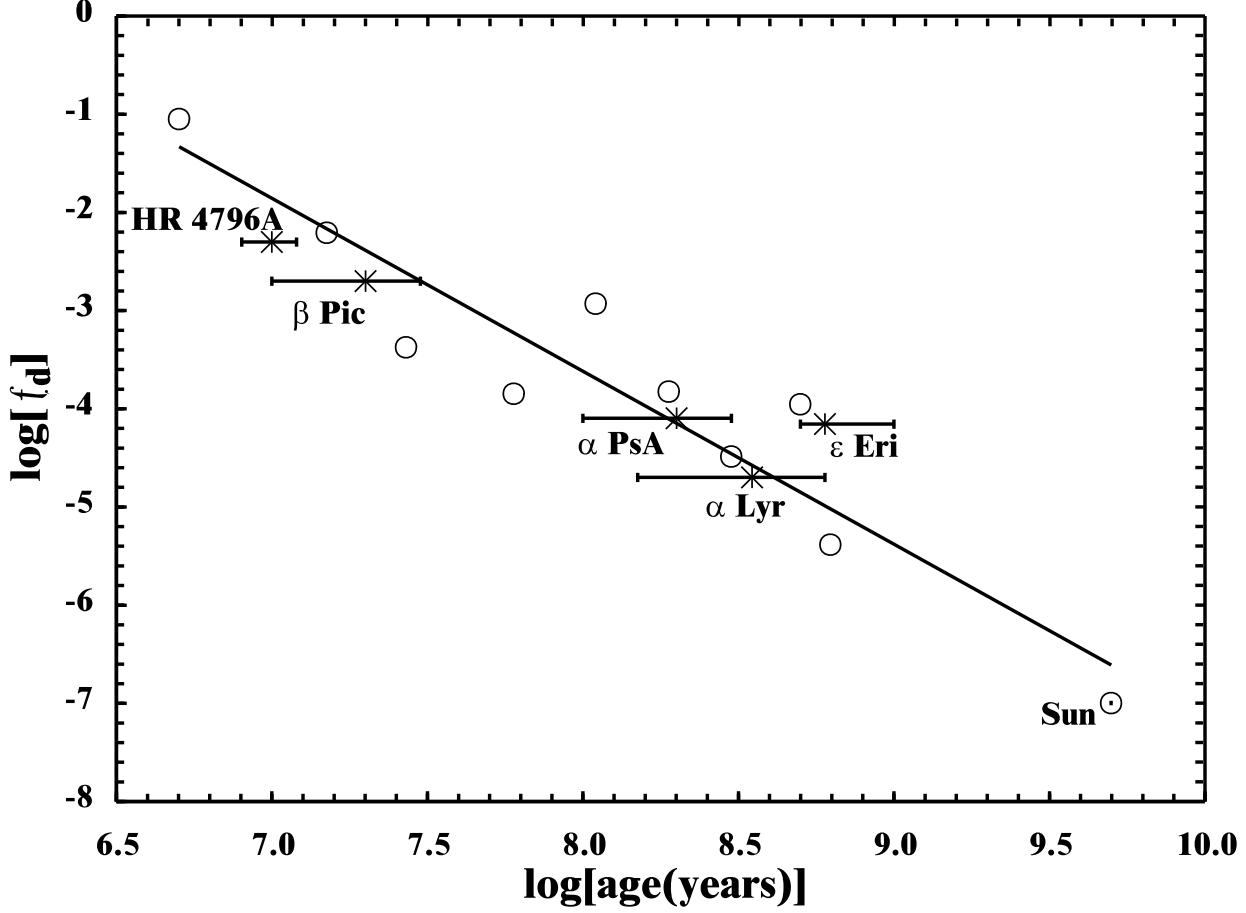


Fig. 2.— Archetypal Vega-phenomenon stars (asterisks) and the Sun are over-plotted on the cluster points (open circles) for comparison (Soderblom & Dappen 1989; Jura et al. 1998; Barrado y Navascues et al. 1999; Holland et al. 1998, and references therein). The position of the Vega-like stars may be regarded as representing a rough upper-envelope of f_a at a given age. The value of f_a plotted for the Sun is based on emission from Zodiacal dust only (≤ 5 AU) and does not include the unknown contribution from outside the orbit of Neptune which could or could not be significant.

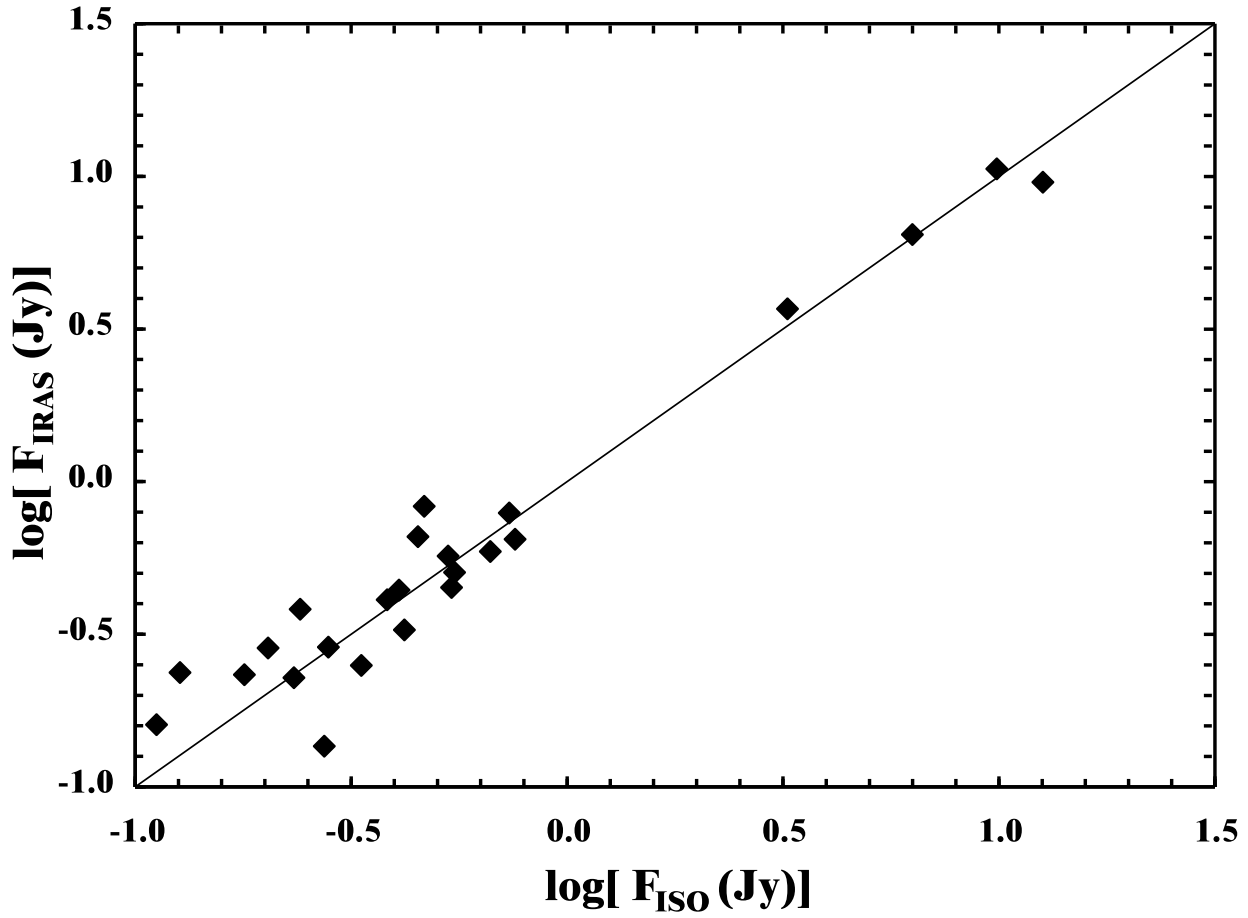


Fig. A1.— Comparison of our calibrated ISO 60 μm observations to IRAS FSC flux densities. The line $F_{\text{ISO}} = F_{\text{IRAS}}$ is plotted for reference.

Table 1. Properties of observed clusters.

Cluster Name	Age (Myr)	ref	Distance (pc)	ref	Number of Targets	Observation Mode	Integration Time (s)
Upper Scorpius	1 – 10	1	145	1	2	raster	53 / raster pt., 473 total
Chamaeleon I a	1 – 20	2	140	3	18	chopped	128 on-target, 128 off-target
Chamaeleon I b	3 – 40	4	150	4	11	raster	40 / raster pt., 346 total
Taurus	10 – 40	5	140	6	2	raster	53 / raster pt., 473 total
α Persei	50	7	185	8	8	raster	40 / raster pt., 346 total
Pleiades	120	7	118	8	13	raster	53 / raster pt., 473 total
Ursa Major	300	9	10 – 40	10	14	raster	53 / raster pt., 473 total
Coma Berenices	500	11	88	11	13	chopped	128 on-target, 128 off-target
Hyades	625	12	46	12	6	raster	53 / raster pt., 473 total
Young Field Stars	60 – 630	13	25 – 125	10	18	chopped	128 on-target, 128 off-target
					8	staring	128 on-target, 128 off-target
					9	raster	53 / raster pt., 473 total
					6	chopped	128 on-target, 128 off-target, 60 μ m 64 on-target, 64 off-target, 100 μ m
					13	raster	46 / raster pt., 410 total

References. — (1) Preibisch & Zinnecker (1999), (2) Lawson et al. (1996), (3) Feigelson et al. (1993), (4) Alcalá et al. (1997), (5) Bouvier et al. (1997), (6) Kenyon, Dobrzycka, & Hartmann (1994), (7) Meynet, Mermilliod, & Maeder (1993), (8) Robichon et al. (1999), (9) Eggen (1973), (10) HIPPARCOS, (11) Odenkirchen, Soubiran, & Colin (1998), (12) Perryman et al. (1998), (13) see Table 2

Table 2. Young Field Star ages.

Object	Age (Myr)	Ref	Object	Age (Myr)	Ref
HD 105	500	1	HD 160934		
HD 1405	60	2	HD 171488	80	6
HD 16884	800	3	HD 175897	100	1
HD 35850	230	4	HD 177996	300	1
HD 36705			HD 180445	160	1
HD 37484	80	3	HD 197890	300	7
HD 54579	160	1	HD 202917	180	1
HD 119022	160	1	HD 209253	400	4
HD 129333	300	5	HD 220140	60	8
HD 134319	500	5			

References. — (1) Henry et al. (1996), (2) Griffin (1992), (3) Favata et al. (1993) (4) This work. (5) Duncan, et al. (1991), (6) Henry et al. (1995) (7) Jeffries (1995), (8) Mantegazza et al. (1992)

Table 3. Targets observed in chopped mode with fluxes and uncertainties.

Target Name	Spectral Type	60 μm (Jy)	RMS Jy	100 μm (Jy)	RMS (Jy)	Target Name	Spectral Type	60 μm (Jy)	RMS Jy	100 μm (Jy)	RMS (Jy)
<i>CHAMAELEON I</i>											
Sz 4	CTTS	0.219	0.038	0.210	0.060	Glass Ia	WTTS	12.970	0.236	7.216	0.445
SZ Cha	CTTS	3.545	0.177	2.546	0.400	HM 19	CTTS	-0.193	2.360	-0.572	3.176
TW Cha	CTTS	0.528	0.078	0.267	0.074	VX Cha	WTTS	0.030	0.063	-0.155	0.193
HM 5	WTTS	0.020	0.055	0.080	0.156	WX Cha	CTTS	0.232	0.045	0.192	0.134
CED 110	WTTS	7.943	0.128	17.995	8.806	GK-1	CTTS	0.566	2.244	2.001	5.104
UX Cha	WTTS	0.024	0.023	0.083	0.091	WY Cha	CTTS	0.303	0.165	0.832	0.548
UZ Cha	WTTS	0.268	0.081	0.229	0.093	CHX 18	WTTS	0.530	0.085	0.372	0.118
Lk Ha 332-17	CTTS	6.715	1.460	8.338	5.474	HM 32	CTTS	0.462	0.029	0.353	0.077
Sz 23	WTTS	0.575	3.033	0.183	6.940	HM Anon	WTTS	0.831	0.104	0.793	0.269
<i>URSA MAJOR</i>											
HD 109011	K2 V	0.019	0.095	-0.037	0.064	HD 124674	F1 V	0.050	0.069	-0.101	0.100
HD 109647	K0	0.052	0.066	0.089	0.032	HD 125451	F5 IV	0.171	0.018	0.004	0.045
HD 110463	K3 V	0.059	0.111	-0.047	0.024	HD 139798	F2 V	0.067	0.022	0.007	0.049
HD 111456	F5 V	0.069	0.040	0.038	0.070	HD 141003	K3 V	0.502	0.326	0.208	0.212
HD 113139	F2 V	0.025	0.044	0.016	0.037	HD 147584	G0 V	0.099	0.072	0.128	0.103
HD 115043	G2 V	0.054	0.023	0.024	0.025	HD 180777	A9 V	0.014	0.053	0.061	0.080
HD 116656	A2 V	0.171	0.022	0.016	0.022						
<i>COMA BERENICES</i>											
HD 105805	A3 V	0.034	0.045	0.011	0.019	HD 107793 ^a	F8 V	0.011	0.018	-0.007	0.008
HD 106103	F5 V	0.005	0.041	0.003	0.008	HD 107887 ^a	F5 V	-0.009	0.033	0.010	0.046
HD 106691	F3 V	0.091	0.091	0.022	0.029	SAO 82286 ^a	G1 V	0.027	0.023	0.008	0.014
HD 106946	F2 V	0.061	0.052	-0.040	0.027	HD 107935 ^a	A7 V	0.085	0.063	0.050	0.052
HD 107067	F9 V	0.170	0.072	0.019	0.061	BD+26 2342	K0 V	0.004	0.031	0.001	0.032
HD 107132	F7 V	0.031	0.042	-0.001	0.027	HD 108102	F8 V	0.150	0.036	0.031	0.033
HD 107131	A7 V	0.044	0.023	0.006	0.018	HD 108154	F8 V	0.051	0.038	-0.014	0.015
HD 107214	G0 V	0.105	0.055	-0.030	0.026	HD 108226 ^a	F6 V	0.086	0.048	-0.007	0.056
HD 107399	G0 V	0.023	0.049	0.023	0.015	Tr 132 ^b	G5 V	-0.048	0.035	0.063	0.034
HD 107583 ^a	G1 V	0.061	0.078	0.000	0.018	HD 108651	A0	0.177	0.055	0.022	0.041
HD 107611 ^a	F6 V	-0.009	0.031	0.013	0.039	SAO 82335	G9 V	-0.089	0.048	0.005	0.022
HD 107685	F5 V	0.100	0.045	0.006	0.012	HD 108967	F6 V	0.051	0.038	0.042	0.019
HD 107700 ^a	A2 V	0.067	0.014	0.025	0.029	HD 109307	A4 V	0.027	0.034	0.009	0.044
	+ G7 III										
<i>YOUNG FIELD STARS</i>											
HD 16884	K5 V	0.137	0.070	0.002	0.046	HD 129333	F8	0.018	0.026	-0.020	0.043
HD 36705	K1 IIIp.	0.008	0.045	0.051	0.029	HD 160934	K7	-0.014	0.025	-0.004	0.031
HD 119022	G2 IV/V	0.047	0.056	0.125	0.091	HD 175897	G0 V	0.043	0.054	-0.041	0.031

Note. — Spectral type information from SIMBAD.

^aStaring Chain observation

^bReplace “Tr” with “Cl Melotte 111” to find in SIMBAD

Table 4. Targets observed in raster mode with fluxes and uncertainties.

Target Name	Spectral Type	60 μm (Jy)	RMS Jy	90 μm (Jy)	RMS (Jy)	Target Name	Spectral Type	60 μm (Jy)	RMS Jy	90 μm (Jy)	RMS (Jy)
<i>UPPER SCORPIUS</i>											
ScoPMS 60	WTTS	0.003	0.008	0.002	0.011	ScoPMS 214	WTTS	0.116	0.008	0.129	0.034
<i>CHAMAELEON I</i>											
RX J0850.1-7554	WTTS	-0.002	0.021	0.020	0.006	RX J1035.8-7859	WTTS	0.013	0.036	0.003	0.011
RX J0853.1-8244	WTTS	0.026	0.019	0.000	0.007	RX J1048.9-7765	WTTS	-0.029	0.030	0.007	0.011
RX J0917.2-7744	WTTS	0.005	0.019	0.008	0.012	RX J1125.8-8456	WTTS	0.019	0.011	-0.001	0.005
RX J0928.5-7815	WTTS	0.003	0.034	0.002	0.012	RX J1203.7-8129	WTTS	-0.006	0.019	-0.002	0.008
RX J0952.7-7933	WTTS	0.005	0.022	0.003	0.009	RX J1225.3-7857	WTTS	0.004	0.009	-0.003	0.009
RX J1007.7-8504	WTTS	0.001	0.019	-0.007	0.007	RX J1325.7-7955	WTTS	-0.017	0.014	0.010	0.014
RX J1009.6-8105	WTTS	0.002	0.018	-0.004	0.009						
<i>TAURUS</i>											
RX J0408.2+1956	WTTS	0.000	0.009	0.009	0.009	RX J0420.4+3123	WTTS	0.012	0.040	0.006	0.016
RX J0409.2+2901	WTTS	0.011	0.032	-0.005	0.021	RX J0423.7+1537	WTTS	0.029	0.026	0.006	0.018
RX J0412.8+2442	WTTS	-0.010	0.013	0.011	0.015	RX J0431.3+2150	WTTS	-0.013	0.021	-0.003	0.015
RX J0415.3+2044	WTTS	0.010	0.014	-0.010	0.019	RX J0457.0+1517	WTTS	-0.002	0.015	0.016	0.009
<i>α PERSEI^a</i>											
HE 061	F0	-0.005	0.017	-0.003	0.015	HE 660	F4 V	-0.007	0.018	-0.018	0.017
HE 143	F8 IV-V	0.025	0.017	0.006	0.012	HE 715	F5 V	0.003	0.013	0.007	0.011
HE 299	F6 V	0.014	0.016	0.011	0.014	HE 733	F6 V	0.009	0.019	0.012	0.018
HE 361	F4 V	0.036	0.010	0.017	0.033	HE 750	F9 V	-0.009	0.020	-0.005	0.014
HE 387	F2 V	0.005	0.009	0.009	0.006	AP 166	G0	0.003	0.012	-0.004	0.014
HE 421	F2 V	0.015	0.008	0.005	0.007	HE 794	F6 V	-0.007	0.025	0.002	0.012
HE 490	F4 V	-0.012	0.012	-0.017	0.015	HE 1101	G4	-0.006	0.021	-0.006	0.015
AP 14	G4	0.001	0.017	0.013	0.013	HE 1160	F7	0.015	0.018	0.004	0.017
HE 621	F4 V	-0.002	0.016	0.019	0.017	HE 1181	G2	-0.012	0.017	0.005	0.009
HE 635	A9 V	0.004	0.012	0.005	0.011						
<i>PLEIADES^b</i>											
HII 1132	F5 V	0.028	0.010	0.026	0.010	HII 2341	G4 V	0.006	0.027	-0.003	0.009
HII 1182	G5 V	-0.011	0.011	-0.006	0.005	HII 2462		0.008	0.023	0.002	0.021
HII 1220	G8 V	0.013	0.018	-0.007	0.014	HII 2506	F8 V	0.002	0.018	0.006	0.010
HII 1593	G6 V	0.015	0.015	0.001	0.015	HII 2786	G0	0.006	0.018	-0.010	0.018
HII 1924	G0 V	-0.011	0.019	0.000	0.015	HII 3163	K2	0.009	0.023	0.038	0.011
HII 2284		-0.013	0.016	0.003	0.022	HII 3179	G0 V	0.019	0.031	0.012	0.005
HII 2311		-0.013	0.021	-0.006	0.024	HII 3197	K3 V	-0.024	0.023	0.010	0.013
<i>URSA MAJOR</i>											
HD 11131	G0 V	0.005	0.004	0.006	0.005	HD 72905	G1 V	0.077	0.014	0.053	0.012
HD 13594	F5 V	0.000	0.004	0.009	0.009	HD 165185	G5 V	0.004	0.004	0.005	0.011
HD 13959	K4 V	0.011	0.007	-0.002	0.007	HD 184960	F7 V	0.050	0.016	0.046	0.012
<i>HYADES</i>											
HD 27429	F3 V	0.001	0.017	-0.007	0.024	HD 28344	G2 V	0.016	0.026	0.007	0.018

Table 4—Continued

Target Name	Spectral Type	60 μ m (Jy)	RMS Jy	90 μ m (Jy)	RMS (Jy)	Target Name	Spectral Type	60 μ m (Jy)	RMS Jy	90 μ m (Jy)	RMS (Jy)
HD 27459	F0 V	0.050	0.013	-0.004	0.012	HD 28677	F4 V	-0.001	0.018	0.002	0.016
HD 27561	F5 V	0.007	0.016	0.017	0.022	HD 28992	G1 V	-0.006	0.018	0.008	0.022
HD 27848	F6 V	0.018	0.025	0.012	0.016	HD 29225	F5 V	0.009	0.022	-0.009	0.016
HD 28205	F8 V	-0.012	0.015	-0.003	0.005						
<i>OTHER</i>											
HD 151044	F8 V	0.088	0.0163	0.103	0.022						
<i>YOUNG FIELD STARS</i>											
HD 105	G0 V	0.143	0.026	0.167	0.008	HD 177996	K1 V	0.019	0.024	0.042	0.017
HD 1405	G5	-0.025	0.016	-0.009	0.009	HD 180445	G8 V	0.032	0.018	0.008	0.012
HD 35850	F7 V	0.049	0.014	0.050	0.012	HD 197890	K0 V	0.002	0.021	0.006	0.009
HD 37484	F3 V	0.115	0.022	0.084	0.011	HD 202917	G5 V	0.050	0.020	0.038	0.015
HD 54579	G0 V	0.000	0.024	-0.003	0.020	HD 209253	F6/F7 V	0.127	0.021	0.107	0.015
HD 134139	G5	0.048	0.019	0.012	0.011	HD 220140	G9 V	-0.001	0.011	-0.006	0.013
HD 171488	G0 V	0.032	0.024	0.017	0.018						

Note. — Spectral type information from SIMBAD.

^anames from: HE = Heckmann, Dieckvoss, & Kox (1956), AP = Stauffer, Hartmann, & Burnham (1985); to find in SIMBAD, replace “HE” with “Cl Melotte 20” and prepend “Cl* Melotte 20” to AP

^bnames from Hertzsprung (1947); to find in SIMBAD, replace “HII” with “Cl Melotte 22”

Table 5. Properties of stars with infrared excess. The list also contains the Chamaeleon I targets observed but not clearly detected for comparison.

Target	SpT	m_v	B-V	$v \sin i$ (km s^{-1})	Distance (pc)	Age (Myr)	Multiplicity
<i>UPPER SCORPIUS</i>							
ScoPMS 214	K0 IV	11.2	1.24	90	160	2	
<i>CHAMAELEON I: detections</i>							
Sz 4	CTTS	140	...	
SZ Cha	CTTS	11.7	1.58	...	140	8	Trinary; sep. $\sim 13''$ and $\sim 5''$
TW Cha	CTTS	13.3	2.02	...	140	20	
CED 110	WTTS	11.3	1.41	75	140	5	
UZ Cha	WTTS	14.9	1.72	...	140	...	
Lk H α 332-17	CTTS	10.7	1.20	30	140	4	Binary; sep. $< 5''$
Glass 1a	WTTS	12.8	1.47	...	140	3	Glass 1b; sep. $\sim 2''$
WX Cha	CTTS	14.8	1.69	...	140	5	Binary; sep. $< 1''$
WY Cha	CTTS	14.0	1.57	...	140	4	
XX Cha	WTTS	15.3	1.53	...	140	40	
CHX 18N	WTTS	12.1	1.31	25	140	8	
HM Anon	WTTS	11.1	1.15	< 16	140	10	Binary; sep. $< 1''$
HM 32	CTTS	13.5	1.44	...	140	5	
RX J0850.1-7554	WTTS	10.6	0.74	45	170 ?	16	
<i>CHAMAELEON I: non-detected or contaminated stars</i>							
HM 5	WTTS	140	...	
UX Cha	WTTS	140	...	
Sz 23	WTTS	140	...	One of at least 3 companions to VW Cha; sep. $\sim 17''$
HM 19	CTTS	140	...	
VX Cha	WTTS	140	...	
GK-1	CTTS	140	...	
<i>α PERSEI</i>							
HE 361	F4 V	9.7	0.43	30	184.2	65	
<i>PLEIADES</i>							
HII 1132	F5 V	9.4	0.45	40	120	120	
HII 3163	K2	12.7	0.96	60	120	120	
<i>URSA MAJOR</i>							
HD 72905	G1 V	5.6	0.62	10	14.3	300	
HD 125451	F5 IV	5.4	0.39	40	26.1	300	Binary; sep. $\sim 160''$
HD 139798	F2 V	5.8	0.35	...	35.7	300	
HD 184960	F7 V	5.7	0.48	7	25.6	300	
<i>COMA BERENICES</i>							
HD 107067	F8	8.7	0.52	6	68.8?	500	SB?
HD 108102	F8	8.2	0.49	35	107.1	500	SB2
HD 108651	A0	6.7	0.22	18	79.0	500	SB2

Table 5—Continued

Target	SpT	m_v	B-V	$v \sin i$ (km s^{-1})	Distance (pc)	Age (Myr)	Multiplicity
<i>HYADES</i>							
HD 27459	F0 V	5.3	0.23	68	47.2	625	
<i>YOUNG FIELD STARS</i>							
HD 105	G0 V	7.5	0.60	13	40.2	500	
HD 35850	F7 V:	6.3	0.50	40	26.8	230	
HD 37484	F3 V	7.2	0.37	42	59.5	80	
HD 134319	G5	8.4	0.64	...	44.3	500	
HD 177996	K1 V	7.9	0.86	4	31.8	300	SB ^a
HD 202917	G5 V	8.7	0.65	12	45.9	180	
HD 209253	F6/F7 V	6.6	0.46	16	30.1	400	
<i>OTHER</i>							
HD 151044	F8 V	6.5	0.54	5	29.4	> 300	

^afrom Soderblom, King, & Henry (1998)

Table 6. PMS Stars with infrared excess in Chamaeleon I and Upper Scorpius. The list also contains the Chamaeleon I targets observed but not clearly detected for comparison.

Target	IRAS Fluxes				ISO Fluxes*		f_d $\times 10^{-4}$	Comment
	12 μm (mJy)	25 μm (mJy)	60 μm (mJy)	100 μm (mJy)	60 μm (mJy)	100 μm (mJy)		
Sz 4	88	142	241	< 4300	219	210	240	
SZ Cha	260	1390	3680	3410	3545	2546	910	1
TW Cha	238	405	450	110 ^a	528	267	480	
CED 110	336	140	< 4930	17130	7945	< 17995	250	2
UZ Cha	112	128	< 210	< 4650	268	229	320	
Lk H α 332-17	2200	3370	6450 ^a	8550 ^a	6715	< 8338	640	3
Glass Ia	10400	14720	9570	< 10400	12970	7216	4120	
WX Cha	500	514	250 ^a	< 15000	232	≤ 200	2240	
WY Cha	< 500	477	830 ^a	20610 ^a	≤ 300	≤ 830	720	4
XX Cha	395	560	590	< 3360	≤ 530	≤ 360	550	5
CHX 18N	≤ 200	≤ 300	...	5
HM Anon	< 250	< 250	790	4640	831	793	130	6
HM 32	93	212	660	1080 ^a	462	353	1010	7
RX J0850.1-7554	< 150	< 200	< 100	< 200	< 62	20 ^b	6.9	8
ScoPMS 214	< 400	< 450	< 600	< 3000	116	129 ^b	27.1	9
Non-detected or contaminated PMS stars								
HM 5	270	129	< 190	< 5390	< 165	< 470	...	10
UX Cha	114	< 150	< 1020	< 82000	< 70	< 272	90	
Sz 23	< 1000	< 1250	≤ 575	≤ 183	...	11
HM 19	≤ 1000	≤ 1550	...	12
VX Cha	< 100	< 100	< 200	< 8000	< 190	< 600	...	13
GK-1	≤ 5500	≤ 22300	...	14

*Photospheric estimates have not been subtracted from the fluxes presented. Upper limits given are 3σ .

^aFrom co-added IRAS data and DECON Weaver & Jones (1992)

^bRaster measurement at 90 μm

Notes –

1. Henning et al. (1993) measured a 1.3mm flux. We included for the purpose of checking calibration of ISO fluxes.
2. Indistinguishable from the nearby reflection nebula in the IRAS beam. At $60\ \mu\text{m}$, our observations indicate a point source. At $100\ \mu\text{m}$ we are only able to place an upper limit to the flux.
3. Henning et al. (1993) measured a 1.3mm flux. At $60\ \mu\text{m}$, our observations indicate a point source. At $100\ \mu\text{m}$ the data appear to be contaminated by flux from the nearby B-type star HD 97048 and we give only an upper limit.
4. Another TTS, CHX 15a falls on one of the source-frame pixels. IRAS detected flux from both objects, and we give an upper limit to the contribution from WY Cha. At $60\ \mu\text{m}$, the total fluxes agree with the IRAS value; at $100\ \mu\text{m}$, cirrus confusion is very high.
5. Originally identified as the source of the far-IR emission detected by IRAS at this position. Subsequent X-ray studies questioned this association, and Walter (1992) considered nearby CHX 18N (also WTTS, separation $\sim 24''$) to be the IR source. In our ISO observations, the two stars fall on different pixels in the source frame. Both pixels show detected emission, and it seems that each star contributes part of the far-IR emission.
6. Has surrounding nebulosity. Appears to be a point source at $60\ \mu\text{m}$, but at $100\ \mu\text{m}$ appears either extended or confused with the nebulosity.
7. Henning et al. (1993) measured a 1.3mm flux. Our measurements at 60 and $100\ \mu\text{m}$ are significantly lower than IRAS co-added data. Evidence for either extension or nebulosity confusion at $100\ \mu\text{m}$.
8. One of the X-ray selected WTTS (Alcala et al. 1995), and it was one of the few confirmed as PMS by detection of lithium (Covino et al. 1997).
9. An X-ray selected WTTS (Walter et al. 1994). It appears quite extended in our data at both wavelengths.
10. Hartigan (1993) notes that this source has essentially disappeared since its first detection.
11. IRAS lists no data for either VW Cha or Sz 23 due to the proximity of the Infrared Nebula. Both stars fall on the same ISOPHOT pixel and we provide an upper limit to their combined fluxes.
12. Contaminated with flux from nearby PSC 11072-7727, the Infrared Nebula.
13. This source appears to be dramatically variable. While Prusti, Whittet, & Wesselius (1992) give near-IR magnitudes, it went undetected by the recent DENIS observations (Cambresy et al. 1998).
14. Contaminated with flux from nearby HD 97300.

Table 7. Open Clusters and Young Field Stars: IRAS PSC and FSC fluxes and new photometry of stars with infrared excess.

Target	IRAS Fluxes				ISO Fluxes*		f_d $\times 10^{-4}$	Comment
	12 μm (mJy)	25 μm (mJy)	60 μm (mJy)	100 μm (mJy)	60 μm (mJy)	90 μm (mJy)		
<i>α PERSEI</i>								
HE 361	< 250	< 250	< 400	< 1800	36	< 100	6.2	
<i>PLEIADES</i>								
HII 1132	224	< 240	< 280	< 2700	28	26	66.0	1
HII 3163	< 100	< 300	< 300	< 2000	< 70	38	93.4	
<i>URSA MAJOR</i>								
HD 72905	885	208	< 180	< 600	77	53	2.8	
HD 125451	717	203	< 160	< 440	170	< 200 ^a	0.77	
HD 139798	497	127	< 240	< 800	62	< 150 ^a	0.33	
HD 184960	605	166	< 170	< 1100	50	46	1.0	
<i>COMA BERENICES</i>								
HD 107067	< 110	< 270	< 280	< 700	170	< 200 ^a	11.5	2
HD 108102	< 150	< 210	< 240	< 600	150	< 200 ^a	5.9	
HD 108651	154	< 200	< 200	< 340	177	< 200 ^a	1.3	
<i>HYADES</i>								
HD 27459	530	< 160	< 350	< 1000	50	< 36	0.95	
<i>YOUNG FIELD STARS</i>								
HD 105	143	167	2.9	
HD 35850	440	80	< 180	< 1930	49	50	0.26	
HD 37484	120	120	130	< 410	115	84	1.6	
HD 134319	48	< 33	1.6	
HD 177996	220	< 170	< 170	< 830	< 72	42	0.47	
HD 202917	50	38	2.5	
HD 209253	290	< 150	140	< 680	127	107	1.0	
<i>OTHER</i>								
HD 151044	321	73	116	< 640	88	100	1.5	3

*Photospheric estimates have not been subtracted from the fluxes presented. Upper limits given are 3σ .

^aChopped upper limit at 100 μm

Note. —

1. IRAS FSC has a 12 μm measurement that is much too high to be photosphere, though there no indication that this has ever been identified as an IR excess source. Our own observations with the UCLA double-beam infrared camera at the Lick 3m Shane telescope show normal magnitudes at J- and K-bands for this star's spectral type.
2. The SB nature of this source is unconfirmed. Odenkirchen et al. (1998) note that the Hipparcos distance for this object is inconsistent with its photometric distance and placing the star at the cluster distance gives values for its space motion that is more consistent with cluster mean values.
3. Once considered an Ursa Major candidate. Please see text.